

From Darkness to Detail: Frequency-Aware SSMs for Low-Light Vision

Eashan Adhikarla
Lehigh University
Bethlehem, Pennsylvania, USA
eaa418@lehigh.edu

Kai Zhang
Lehigh University
Bethlehem, Pennsylvania, USA
kaz321@lehigh.edu

Gong Chen
Lenovo Research
Chicago, Illinois, USA
gochen24@lenovo.com

John Nicholson
Lenovo Research
Raleigh, North Carolina, USA
jnichol@lenovo.com

Brian D. Davison
Lehigh University
Bethlehem, Pennsylvania, USA
bdd3@lehigh.edu

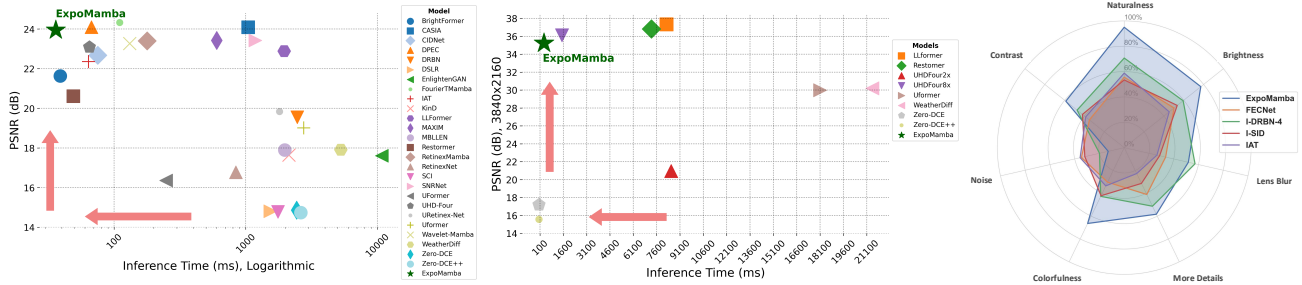


Figure 1. [Left: 400x600; Middle: 3840x2160] Logarithmic Scatter Plot of Inference Time vs. PSNR. Baselines that used ground-truth mean information to produce metrics were reproduced without such information for fairness, [Right:] Spider chart with comparison of ExpoMamba outputs with other SOTA light-weight models on perceptual realism.

Abstract

*Low-light image enhancement remains a persistent challenge in computer vision, where state-of-the-art models are often hampered by hardware constraints and computational inefficiency, particularly at high resolutions. While foundational architectures like transformers and diffusion models have advanced the field, their computational complexity limits their deployment on edge devices. We introduce **ExpoMamba**, a novel architecture that integrates a frequency-aware state-space model within a modified U-Net. ExpoMamba is designed to address mixed-exposure challenges by **decoupling the modeling of amplitude (intensity) and phase (structure)** in the frequency domain. This allows for targeted enhancement, making it highly effective for real-time applications, including downstream tasks like object detection and segmentation. Our experiments on six benchmark datasets show that ExpoMamba is up to **2-3x** faster than competing models and achieves a **6.8% PSNR improvement**, establishing a new state-of-the-art in efficient, high-quality low-light enhancement. Source code: github.com/eashanadhikarla/ExpoMamba.*

1. Introduction

Enhancing low-light images is crucial for applications ranging from consumer gadgets like phone cameras [45, 50] to sophisticated surveillance systems [27, 68, 88]. Traditional techniques [15, 38, 40, 64, 69] often struggle to balance processing speed and image quality, particularly with high-resolution, resulting in noise and color distortion in scenarios that demand fast processing such as mobile photography and real-time video streaming.

Limitations of Current Approaches. Foundation models have revolutionized computer vision, including low-light image enhancement, by introducing advanced architectures that model complex relationships within image data. In particular, transformer-based [1, 9, 80, 104] and diffusion-based [79, 82, 102] low-light techniques have made significant strides. However, the sampling process requires a computationally intensive iterative procedure, and the quadratic runtime of self-attention in transformers makes them unsuitable for real-time use on edge devices where limited processing power and battery constraints pose challenges. Innovations such as linear attention [37, 67, 77], self-attention approximation, windowing,

striding [39, 94], attention score sparsification [48], hashing [12], and self-attention operation kernelization [11, 37, 53] have aimed to address these complexities, but often at the cost of increased computation errors compared to simple self-attention [17, 18]. (See details in Section 2)

Purpose. With the rising need for better images, advanced small camera sensors in edge devices have made it more common for customers to capture high-quality images and use them in real-time applications like mobile, laptop, and tablet cameras [58]. However, they all struggle with non-ideal and low-lighting conditions in the real world. Our objective is to achieve a practical balance between perceptual quality (e.g., CIDNet [19]) and runtime efficiency (e.g., IAT [13], Zero-DCE++ [42]), while also demonstrating improvements on downstream vision tasks—such as object detection and segmentation—that are critical for machine perception in autonomous driving and robotic systems operating under poor lighting.

Contributions. Our contributions are summarized as: (i) We introduce the use of Mamba for efficient low-light image enhancement (LLIE), specifically focusing on mixed exposure challenges, where underlit (insufficient brightness) and overlit (excessive brightness) exist in the same image frame. (ii) We propose a novel Frequency State Space Block (FSSB) that combines two distinct 2D-Mamba blocks for decoupled modeling of amplitude and phase, allowing the model to enhance brightness and structural consistency separately—critical for perceptual quality in low-light scenes. (iii) We describe a novel dynamic batch training scheme to improve robustness of multi-resolution inference in our proposed model. (iv) We implement dynamic processing of the amplitude component to highlight distortion (noise, illumination) and the phase component for image smoothing and noise reduction.

2. Related Work

2.1. Addressing Performance Bottlenecks

The evolution of LLIE has been driven by a cycle of architectural innovation. Although CNNs established the power of data-driven approaches, their inherently local receptive fields struggle to model global illumination inconsistencies. This led to the adoption of Transformers (LLFormer [80], IAT [13], IPT [9], Fourmer [104], LYT-Net [6]), whose self-attention mechanism excels at capturing long-range dependencies, achieving state-of-the-art results in models like Retinexformer [8]. However, this power comes at a steep cost: the “quadratic bottleneck.” The self-attention mechanism scales with a complexity of $O(n^2)$ to image patch count, making Transformers prohibitively slow and memory-intensive for high-resolution imagery and real-time deployment on edge devices.

This fundamental efficiency challenge necessitated a new paradigm. State-Space Models (SSMs), particularly

the Mamba architecture [22], have emerged as the definitive solution. Mamba-based models can capture global context and long-range dependencies with linear-time complexity, $O(n)$, matching the efficiency of RNNs while retaining the parallelizable training of CNNs and the expressive power of Transformers. This breakthrough resolves a long-standing architectural trade-off, paving the way for a new generation of efficient and powerful restoration models.

2.2. Mamba-based Low-Light Image Enhancement

Mamba’s introduction has spurred a new generation of LLIE models. Many are *retinex-inspired frameworks*, including deep unfolding networks like LLEMamba [98], backbone replacements like RetinexMamba [5], artifact-reducing models like MambaLLIE [86], and efficiency-focused variants like EffRetMamba [99]. Other works explore novel paradigms, from the semantic scanning of BSMamba [97] to the real-time residual prediction of ResVMUNetX [78] and the data-efficient learning of Semi-LLIE [44]. A third group modifies Mamba’s interaction space by combining it with frequency or wavelet transforms, as seen in Fourier TMamba [59], Wavelet-Mamba [70] and WaveMamba [106].

Despite these innovations, prior works largely treat Mamba as a backbone replacement, a sequence re-ordering pre-processor, or a component within existing spatial frameworks. **ExpoMamba** innovates at a more fundamental level by operating directly in the frequency domain. Our Frequency State Space Block (FSSB) is the first to employ a dual-branch Mamba architecture to explicitly and independently process amplitude (illumination) and phase (structure). This principled, signal-level decomposition enables fine-grained control, distinguishing our method from those reliant on high-level theories like Retinex or input-reordering schemes. By synergizing the global nature of the Fourier transform with Mamba’s linear-time modeling, ExpoMamba establishes a new and effective pathway for LLIE. Additional related work is in **Appx. A**.

3. Exposure Mamba

Building upon recent advances in efficient sequence modeling [22, 84, 105], we propose *ExpoMamba*—a hybrid architecture designed for low-light image enhancement that fuses frequency-aware and spatial learning. The model adopts a modified U-Net structure (combination of $U^2 - Net$ [62] and M-Net [56]), where each encoder-decoder block combines a traditional spatial convolutional unit with a Frequency State Space Block. Each FSSB incorporates two Visual SSM (VSSM) modules, based on the Mamba architecture [22], which independently process frequency-transformed amplitude and phase features. More details are deferred to Section 3.1; here we emphasize that this hybrid design allows ExpoMamba to efficiently capture multi-

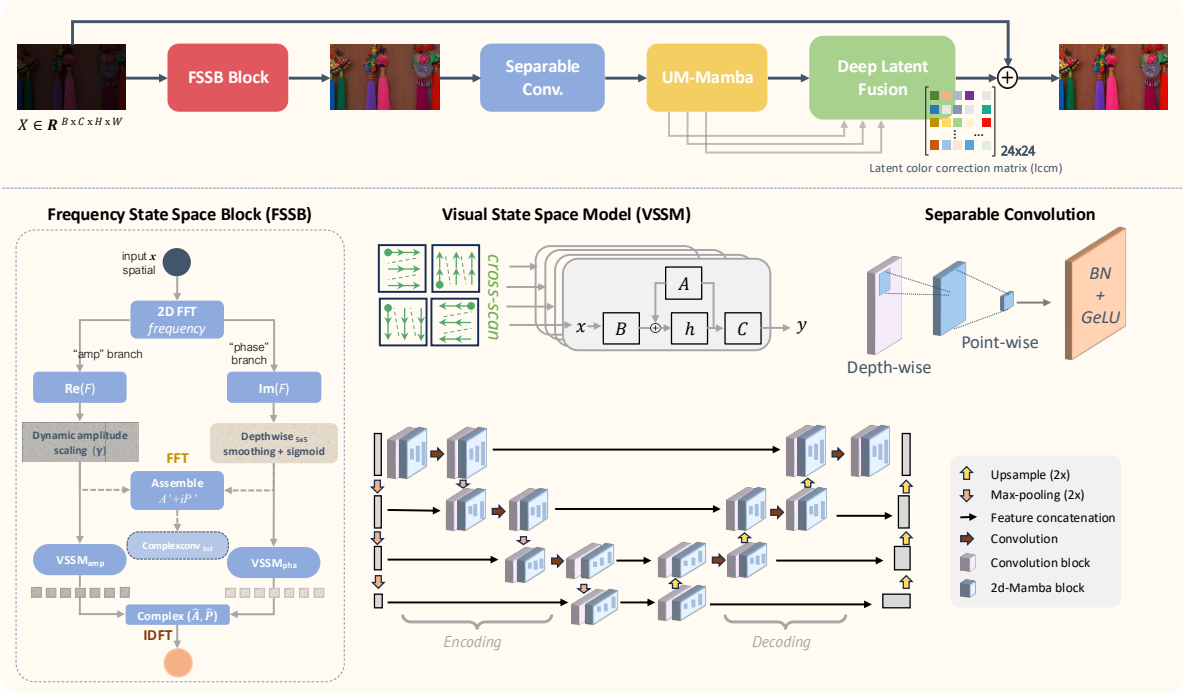


Figure 2. **Overview of the ExpoMamba Architecture.** The diagram illustrates the information flow through the *ExpoMamba* model. The architecture efficiently processes sRGB images by integrating convolutional layers, 2D-Mamba blocks, and deep supervision mechanisms to enhance image reconstruction, particularly in low-light conditions.

scale contextual cues critical for restoring under- and over-exposed regions. The overall pipeline employs a 2D scanning strategy on sRGB images with each block performing operations using a convolutional and encoder-style SSM ($x(t) \in \mathbf{R} \rightarrow y(t) \in \mathbf{R}$)¹.

3.1. Frequency State Space Block (FSSB)

The Frequency State Space Block (FSSB) integrates state-space modeling with frequency decomposition to enhance low-light images. Unlike conventional spatial-only models that operate on entangled signal content [101, 104], FSSB performs a Fourier decomposition of the input into amplitude and phase components, allowing for distinct processing of luminance and structural cues. This separation is critical: amplitude carries information about illumination and contrast, while phase governs edges and object boundaries—features tightly correlated with human visual perception [89, 104].

The FSSB (as in Fig. 2) initiates its processing by transforming the input image I into the frequency domain. We specifically choose the Fourier transform because its global, harmonically ordered spectral decomposition aligns with Mamba’s architectural strengths in efficiently processing continuous 1D sequences. This allows our model to se-

lectively modulate low-frequency bands, which carry most of the critical illumination and structure information, while handling high-frequency noise—a synergy not as readily achieved with more localized transforms like wavelets.

$$\mathbf{F}(u, v) = \iint \mathbf{I}(x, y) e^{-i2\pi(ux+vy)} dx \cdot dy \quad (1)$$

where $\mathbf{F}(u, v)$ denotes the frequency domain representation of the image, and (u, v) are the frequency components corresponding to the spatial coordinates (x, y) . This transformation allows for the isolation and manipulation of specific frequency components, which is particularly beneficial for enhancing details and managing noise in low-light images. By decomposing the image into its frequency components, we can selectively enhance high-frequency components to improve edge and detail clarity while suppressing low-frequency components that typically contain noise [41, 103]. This selective enhancement and suppression improve the overall image quality.

The core of the FSSB comprises two 2D-Mamba (Visual-SSM) blocks to process the amplitude and phase components separately. While the VSSM architecture is structurally shared for implementation simplicity, note that the model parameters for the amplitude and phase branches are learned **independently**. This enables each branch to specialize in its respective task: correcting illumination and

¹A state space model is a type of sequence model that transforms a one-dimensional sequence via an implicit hidden state.

noise via the amplitude stream, and preserving fine-grained structural detail via the phase stream. These blocks model the state space transformations as follows:

$$\mathbf{h}[t + 1] = \mathbf{A}[t] \cdot \mathbf{h}[t] + \mathbf{B}[t] \cdot x[t] \quad (2)$$

$$\mathbf{y}[t] = \mathbf{C}[t] \cdot \mathbf{h}[t] \quad (3)$$

Here, $\mathbf{A}[t]$, $\mathbf{B}[t]$, and $\mathbf{C}[t]$ are the state matrices that adapt dynamically based on the input features, and $h[t]$ represents the state vector at time t . $\mathbf{y}[t]$ represents processed feature at time t , capturing the transformed information from the input features. This dual-pathway setup within the FSSB processes amplitude and phase in parallel.

After processing through each of the VSS blocks, the modified amplitude and phase components are recombined and transformed back to the spatial domain using the inverse Fourier transform:

$$\hat{\mathbf{I}}(x, y) = \iint \hat{\mathbf{F}}(u, v) e^{-i2\pi(ux+vy)} du \cdot dv \quad (4)$$

where $\hat{\mathbf{F}}(u, v)$ is the processed frequency domain representation in the latent space of each M-Net block. This method preserves the structural integrity of the image while enhancing textural details that are typically lost in low-light conditions, removing the need of self-attention mechanisms that are widely seen in transformer-based pipelines [71]. The FSSB also integrates hardware-optimized strategies similar to those employed in the Vision-Mamba architecture [22, 105] such as scan operations and kernel fusion, reducing memory IOs, facilitating efficient data flow between the GPU’s memory hierarchies. This optimization significantly reduces computational overhead by a factor of $O(N)$ speeding the operation by 20 – 40 times [22], enhancing processing speed for real-time applications. This can be seen in Fig. 1, where increasing the resolution size or input length significantly widens the inference time gap, primarily because the multihead attention mechanism in transformer-based models has a computational complexity of $O(N^2)$.

Within the FSS Block, the amplitude $\mathbf{A}(u, v)$ and phase $\mathbf{P}(u, v)$ components extracted from $\mathbf{F}(u, v)$ are processed through dedicated state-space models. These models, adapted from the Mamba framework, are particularly tailored (dynamic adaptation of state matrices (\mathbf{A} , \mathbf{B} , \mathbf{C} ; details in **Appx. D**) based on spectral properties and the dual processing of amplitude and phase components²) to enhance information across frequencies, effectively addressing the typical loss of detail in low-light conditions.

Amplitude and Phase Component Modeling. Each component $\mathbf{A}(u, v)$ and $\mathbf{P}(u, v)$ undergoes separate but parallel processing paths, modeled by: $s_{t+1} = \mathbf{A}(s_t) + \mathbf{B}\mathbf{F}(\mathbf{x}_t)$, $y_t = \mathbf{C}s_t$; where, s_t denotes the state at time t ,

²refer to FSSB module in Section 4.2.

$\mathbf{F}(\mathbf{x}_t)$ represents the frequency-domain input at time t (either amplitude or phase), and \mathbf{A} , \mathbf{B} , \mathbf{C} are the state-space matrices that dynamically adapt during training.

3.2. Phase Manipulation

For an image $I(x, y)$, its Fourier transform $\mathbf{F}(u, v) = \mathbf{A}(u, v)e^{i\phi(u, v)}$, where $\mathbf{A}(u, v)$ is the amplitude and $\phi(u, v)$ is the phase. A uniform shift $\Delta\phi$ to the phase results in a modified image $I'(x, y)$. The derivation is as follows:

$$I'(x, y) = \iint \mathbf{A}(u, v) e^{i(\phi(u, v) + \Delta\phi)} e^{i2\pi(ux+vy)} du dv \quad (5)$$

$$= \iint \mathbf{A}(u, v) e^{i\phi(u, v)} e^{i\Delta\phi} e^{i2\pi(ux+vy)} du dv \quad (6)$$

$$= e^{i\Delta\phi} \iint \mathbf{A}(u, v) e^{i\phi(u, v)} e^{i2\pi(ux+vy)} du dv \quad (7)$$

$$= (\cos(\Delta\phi) + i \sin(\Delta\phi)) I(x, y) \quad (8)$$

This formulation reveals that a uniform phase shift transforms the spatial structure of the image. As prior studies show [89], human vision is highly sensitive to phase variations. By adaptively modifying the phase, our model preserves and refines scene structure (e.g., edges, contours), while the amplitude branch handles illumination and contrast. We use phase offset as a single scalar per FSSB stage, denoted $\Delta\phi_s$, learned during training and applied uniformly to all (u, v) . For stability it is bounded to $[-\Delta\phi_{\max}, \Delta\phi_{\max}]$ with a smooth clipping (extended details in **Appx. B**).

3.3. Algorithm

The pseudocode found in Algorithm 1 presents the details of ExpoMamba training with FSSB blocks.

Algorithm 1 Concise ExpoMamba Training w/ FSSB

Require: dataset \mathcal{D} , epochs E , model params θ (FSSB \rightarrow HDR \rightarrow ComplexConv)

- 1: **for** $I \in \mathcal{D}$ **do**
- 2: $(A, P) \leftarrow \text{FFT}(I)$
- 3: $(A'', P'') \leftarrow \text{VSSM}(A, P)$
- 4: $\hat{I} \leftarrow \text{IFFT}(A'' + iP'')$
- 5: **end for**
- 6: **for** $e = 1$ **to** E **do**
- 7: **for** mini-batch \mathcal{B} **do**
- 8: $\hat{\mathcal{B}} \leftarrow \text{ComplexConv}(\text{HDR}(\text{FSSB}(\mathcal{B})))$
- 9: $\theta \leftarrow \theta - \eta \nabla_{\theta} \mathcal{L}(\hat{\mathcal{B}}, \mathcal{B})$
- 10: **end for**
- 11: **end for**
- 12: **return** θ

A detailed version can be found in Supp. 2.

Latent Space Color Correction Matrix (LCCM) Why latent instead of image space. (1) *Precision.* Latent tensors are floating point, while image space is typically 8 to 10 bit per channel. Applying color mixing in latent space avoids rounding and clipping, so small corrections can be learned and accumulated without staircasing. (2) *Expressivity.* We act on a C channel feature basis rather than only RGB. This enables a $C \times C$ CCM (we use $C=24$) that generalizes the standard 3×3 matrix and can model sensor and ISP shifts as well as scene dependent tints and cross-channel couplings. (3) *Semantics and stability.* Latent features carry edges, textures, and mixed exposure cues that are attenuated in pixels. Operating in this space makes the correction more stable under low light noise and uneven illumination.

Formulation and placement. Given $X \in \mathbb{R}^{C \times H \times W}$, the LCCM is a per-pixel linear map $W \in \mathbb{R}^{C \times C}$ with bias b ,

$$Y(:, h, w) = W X(:, h, w) + b, \quad (9)$$

implemented as a 1×1 convolution. We initialize $W=I_C$, $b=0$, and add a small penalty $\lambda \|W - I_C\|_F^2$ to discourage unnecessary drift. We place one LCCM before HDR gating in each decoder FSSB and a final LCCM before the output head. The cost is $O(C^2HW)$; with $C=24$ the per-pixel multiplies are 576, which is negligible relative to surrounding blocks.

As noted in ablation study 5, the LCCM corrects sensor and ISP color shifts while reducing banding and quantization artifacts, aligning with ExpoMamba’s goal of high fidelity without relying on post-hoc RGB fixes.

Feature Recovery in FSSB. We implement an HDR gate in feature space. Overexposed activations are detected with a soft mask $M = \sigma(k(Y - \tau))$ and corrected using a gentle tone curve $T(x) = \log(1 + sx)$ or a learned CSRNet variant. We blend only where M is high: $\tilde{x} = (1 - M) \circ x + M \circ T(x)$. This layer sits at the end of each FSSB and before the final output head, which attenuates halos and blooming while preserving detail. Unless stated otherwise we use $\tau = 0.90$. Figure 3 compares the parametric and CSRNet+ options.

We leverage the ComplexConv function from complex networks as introduced by Trabelsi et al. [72]. This function is incorporated into our model to capture and process additional information beyond traditional real-valued convolutions. Specifically, the ComplexConv function allows the simultaneous manipulation of the amplitude and phase information in the frequency domain, which is essential to preserve the integrity of textural details in low-light images. The dual processing of amplitude and phase ensures that each component is optimized separately. Tone mapping and ComplexConv have proven effective in overcoming limitations of traditional image processing techniques [28, 51]. We integrate these methods into our FSS design



Figure 3. The effectiveness of various HDR tone mapping layers inside the FSS block. CSRNet+ with shrunken conditional blocks and dilated convolutions lessens overexposed artifacts.

Table 1. Comparing four popular metrics such that every column showcases the top three methods; **dark**, **medium**, and **light** shades of blue representing the best, second best, and third best models among the proposed and all popular SOTA models.

Methods	LOLv1			LOLv2 (Real Captured)			Inference time (ms)
	PSNR \uparrow	SSIM \uparrow	LPIPS \downarrow	PSNR \uparrow	SSIM \uparrow	LPIPS \downarrow	
Retinex [‡]	16.774	0.462	0.417	17.715	0.652	0.436	4493
MIRNet	24.138	0.830	0.250	20.020	0.82	0.233	1795
EnlightenGAN [‡]	17.606	0.653	0.372	18.676	0.678	0.364	-
ReLLIE [‡]	11.437	0.482	0.375	14.400	0.536	0.334	3.500
RUAS [‡]	16.405	0.503	0.364	15.351	0.495	0.395	15.51
DDIM	16.521	0.776	0.376	15.280	0.788	0.387	1213
CDEF	16.335	0.585	0.407	19.757	0.63	0.349	-
SCI	14.784	0.525	0.366	17.304	0.54	0.345	1755
URetinex-Net	19.842	0.824	0.237	21.093	0.858	0.208	1804
SNRNet [‡]	23.432	0.843	0.234	21.480	0.849	0.237	72.16
Uformer*	19.001	0.741	0.354	18.442	0.759	0.347	901.2
Restormer*	20.614	0.797	0.288	24.910	0.851	0.264	513.1
Palette [♣]	11.771	0.561	0.498	14.703	0.692	0.333	168.5
UHDFour [‡]	23.093	0.821	0.259	21.785	0.854	0.292	64.92
WeatherDiff [♣]	17.913	0.811	0.272	20.009	0.829	0.253	5271
GDP [♣]	15.896	0.542	0.421	14.290	0.493	0.435	-
DiffLL [♣]	26.336	0.845	0.217	28.857	0.876	0.207	157.9
CIDNet [‡]	23.090	0.851	0.085	23.220	0.863	0.103	-
LLformer*	22.890	0.816	0.202	23.128	0.855	0.153	1956
ExpoMamba	22.870	0.845	0.215	23.000	0.860	0.203	36.00
ExpoMamba_{da}	23.092	0.847	0.214	23.131	0.868	0.224	38.00
ExpoMamba_{gt}	25.770	0.860	0.212	28.040	0.885	0.232	36.00

*"da" - Dynamic adjustment. (refer Section-4.2) / "gt" - With ground-truth mean.

to address adverse lighting conditions in low-light environments. The input components in the frequency representation are processed through dynamic amplitude scaling and phase continuity layer as shown in Fig. 2. As claimed by Fourmer [104], we have determined that the primary source of image degradation is indeed amplitude, specifically in the area between the amplitude and phase division within the image. Moreover, we found the amplitude component primarily affects brightness of the image, directly impacting the visibility and the sharpness of the features within the image. However, the phase component encodes the positional information of these features, defining the structure and the layout of the image. The phase component of the image has previously been found to have a close relation with perceptual analysis [89]. Along those lines, we show that the human visual system is more sensitive to changes in phase rather than amplitude (see Section 3.2).

3.4. Multi-modal Feature Learning

The inherent complexity of low-light images, where both underexposed and overexposed elements coexist, necessi-

tates a versatile approach to image processing. Traditional methods, which typically focus either on spatial details or frequency-based features, fail to adequately address the full spectrum of distortions encountered in such environments. By contrast, the hybrid modeling approach of ExpoMamba leverages the strengths of both the spatial and frequency domains, facilitating a more comprehensive and nuanced enhancement of image quality.

Operations like the Fourier transform offer the ability to isolate distortion modes by frequency, allowing ExpoMamba to denoise brightness artifacts via amplitude manipulation and preserve fine-grained structures via phase-aware reconstruction. This domain provides a global view of the image data, allowing for the manipulation of features that are not easily discernible in the spatial layout. Simultaneously, the spatial domain is critical for maintaining the local coherence of image features, ensuring that enhancements do not introduce unnatural artifacts. Finally, the hybrid-modeled features pass through deep supervision, where we combine ExpoMamba’s intermediate layer outputs, apply a color correction matrix (CCM) in the latent dimensions during deep supervision, and pass through the final layer.

While most LLIE approaches focus solely on perceptual quality, ExpoMamba is explicitly evaluated on downstream tasks relevant to autonomous systems, such as object detection and scene parsing. Our frequency-aware hybrid design preserves structural integrity and suppresses noise, which are essential to improve downstream model performance (e.g., YOLOv3 and DeepLab-V3+) on low-light images. This bridges the gap between low-level enhancement and high-level vision reliability in real-world applications.

4. Experiments and Implementation Details

We evaluate ExpoMamba through a series of experiments. We begin by outlining the datasets used, experimental setup, followed by a comparison of our method against state-of-the-art techniques using four quantitative metrics. We also perform a detailed ablation study in Tab. 5/Sec. 4.2.

4.1. Datasets

We tested the efficacy of our model on four datasets: **(1) LOL** [85]. LOLv2 [90] is divided into real and synthetic subsets. The training and testing sets are split into 485/15, 689/100, and 900/100 on LOLv1, LOLv2-real, and LOLv2-synthetic with $3 \times 400 \times 600$ resolution images. **(2) LOL4K** is an ultra-high definition dataset with $3 \times 3840 \times 2160$ resolution images, containing 8,099 pairs of low-light/normal-light images, split into 5,999 pairs for training and 2,100 pairs for testing. **(3) SICE** [7] includes 4,800 images, real and synthetic, at various exposure levels and resolutions, divided into training, validation, and testing sets in a 7:1:2 ratio. **(4) ExDark** [52] is a real-world object detection dataset comprising 7,363 low-light images from 12 object categories, with annotated bounding boxes. We follow an 80/20

Table 2. Evaluation on the UHD-LOL4K dataset. †, ‡, §, △, and ★ denote supervised CNN, unsupervised CNN, zero-shot, and transformer-based models, respectively. We use dynamic adjustment for both ‘s’ and ‘l’ ExpoMamba models during inference.

Methods	UHD-LOL4K			
	PSNR ↑	SSIM ↑	LPIPS ↓	MAE ↓
SRIE [†] [21]	16.7730	0.8365	0.1495	0.1416
MSRCR [†] [36]	12.5238	0.8106	0.2136	0.2039
RetinexNet [‡] [85]	21.6702	0.9086	0.1478	0.0690
DSLR [‡] [46]	27.3361	0.9231	0.1217	0.0341
KinD [‡] [100]	18.4638	0.8863	0.1297	0.1060
Z.DCE [§] [23]	17.1873	0.8498	0.1925	0.1465
Z.DCE++ [§] [42]	15.5793	0.8346	0.2223	0.1701
RUAS [△] [49]	14.6806	0.7575	0.2736	0.1690
ELGAN [△] [35]	18.3693	0.8642	0.1967	0.1011
Uformer★ [83]	29.9870	0.9804	0.0342	0.0376
Restormer★ [95]	36.9094	0.9881	0.0226	0.0117
LLFormer★ [80]	37.3340	0.9862	0.0200	0.0116
UHD-Four [43]	35.1010	0.9901	0.0210	-
ExpoMamba _s	28.3300	0.9730	0.0820	0.0315
ExpoMamba _l	35.2300	0.9890	0.0630	0.0451

Table 3. Performance comparison with recent Mamba-based LLIE models on LOLv1 and LOLv2 datasets.

Model	LOLv1		LOLv2	
	PSNR ↑	SSIM ↑	PSNR ↑	SSIM ↑
RetinexMamba [5]	24.02	0.827	22.45	0.844
Fourier TMamba [59]	24.33	0.845	22.41	0.860
Wavelet-Mamba [70]	23.27	0.851	22.49	0.869
MambaLLIE [86]	-	-	22.95	0.847
EffRetMamba [99]	23.65	0.837	22.32	0.841
ExpoMamba _{gt}	25.77	0.860	28.04	0.885

training/test split and resize images to 608×608 resolution for YOLOv3-based detection. **(5) ACDC** [66] is a nighttime urban scene segmentation dataset containing 1,006 images. We fine-tune DeepLab-V3+ on its night-time training subset and evaluate on the validation set using mIoU (mean Intersection over Union).

4.2. Experimental setting

The proposed network is a single-stage end-to-end training model. The patch sizes are set to 128×128 , 256×256 , and 324×324 with checkpoint restarts and batch sizes of 8, 6, and 4, respectively, in consecutive runs. For dynamic patch training, we use different patch sizes simultaneously. To improve robustness across input resolutions, we adopt a dynamic patch training strategy randomizing patch sizes across batches. This enhances scale-invariance and supports efficient multi-resolution inference (more details in Appx. E). The optimizer is RMSProp with learning rate of 1×10^{-4} , weight decay of 1×10^{-7} , and momentum of 0.9. A linear warm-up cosine annealing scheduler with 15 warm-up epochs is used, starting with a learning rate of 1×10^{-4} . All experiments are conducted on NVIDIA A10 GPU. For model configuration details see Tab. 7.

For downstream tasks, we follow the configurations used in IAT [13] and ILE-YOLO [81]. For object detection, we



Figure 4. Qualitative comparison of ExpoMamba and baselines on the LOLv1 dataset. Results demonstrate structural fidelity and color balance under mixed lighting conditions.

Table 5. Ablation of ExpoMamba FSSB components.

Config	FSSB	HDR	CSRNet ⁺	HDR _{out}	DA	PSNR / SSIM
Conv baseline	×	×	×	×	×	18.978 / 0.815
+ FSSB only	✓	×	×	×	×	19.787 / 0.828 (+0.809 / +0.013)
+ HDR only	×	✓	×	×	×	22.459 / 0.836 (+3.481 / +0.021)
+ CSRNet ⁺ only	×	×	✓	×	×	20.576 / 0.823 (+1.598 / +0.008)
+ FSSB + HDR	✓	✓	×	×	×	24.878 / 0.841 (+5.900 / +0.026)
FSSB + HDR + DA + CSRNet ⁺	✓	✓	✓	×	✓	25.110 / 0.845 (+6.132 / +0.030)
FSSB + HDR + HDR _{out} + DA	✓	✓	×	✓	✓	25.640 / 0.860 (+6.662 / +0.045)

Table 6. Comparative performance over SICE-v2 [7] datasets. Our ‘s’: smallest model outperforms all the baselines.

Method	SICE-v2						#params
	Underexposure		Overexposure		Average		
	PSNR ↑	SSIM ↑	PSNR ↑	SSIM ↑	PSNR ↑	SSIM ↑	
RetinexNet [85]	12.94	0.5171	12.87	0.5252	12.90	0.5212	0.84M
URetinexNet [87]	12.39	0.5444	7.40	0.4543	12.40	0.5496	1.32M
DeepLPE [75]	16.21	0.6807	11.98	0.5967	14.10	0.6387	7.79M
SID-L [30]	19.43	0.6644	17.00	0.6495	18.22	0.6570	11.56M
RUAS [47]	16.63	0.5589	4.54	0.3196	10.59	0.4394	0.0014M
SCI [55]	17.86	0.6401	4.45	0.3629	12.49	0.5051	0.0003M
MSEC [2]	19.62	0.6512	17.59	0.6560	18.58	0.6536	7.04M
LCDPNet [74]	17.45	0.5622	17.04	0.6463	17.25	0.6043	0.96M
DRBN [91]	17.96	0.6767	17.33	0.6828	17.65	0.6798	0.53M
DRBN-ERL+ENC [32]	22.06	0.7053	19.50	0.7205	20.78	0.7129	0.58M
ELCNet [33]	22.05	0.6893	19.25	0.6872	20.65	0.6861	0.018M
ELCNet+ERL [32]	22.14	0.6908	19.47	0.6982	20.81	0.6945	0.018M
FECNet [29]	22.01	0.6737	19.91	0.6961	20.96	0.6849	0.15M
FECNet+ERL [32]	22.35	0.6671	20.10	0.6891	21.22	0.6781	0.15M
IAT [13]	21.41	0.6601	22.29	0.6813	21.85	0.6707	0.090M
ExpoMamba	22.59	0.7161	20.62	0.7392	21.61	0.7277	41M

train 608×608 with an 80/20 split using SGD (momentum=0.9, weight decay= 1×10^{-4} , learning rate= 1×10^{-3} , batch size=8). For segmentation, DeepLab-V3+ (ResNet-101 backbone, pre-trained on Cityscapes) is fine-tuned on ACDC-night training images using SGD (initial learning rate=0.05, weight decay= 5×10^{-4}). Performance was collected on raw and enhanced inputs using mean Average Precision (mAP) and mIoU.

Baselines. We use official code for MIRNet, Restormer, LLFormer, URetinex-Net, and DiffLL. MIRNet, Restormer, and LLFormer are retrained on LOL-v1/v2 and SICE with their recommended losses and schedulers. URetinex-Net and DiffLL use released weights due to training cost. When retraining, we adopt each paper’s epochs, augmentations, and loss composition; if absent, we train for 300 epochs with cosine decay and early stop on PSNR.

Table 4. Experimental results on low-light object detection (ExDark) and segmentation (ACDC) tasks.

Methods	ExDark Detection		ACDC Segmentation	
	mAP ↑	time (s) ↓	mIOU ↑	time (s) ↓
YOLOv3 [63]	76.4	0.033	63.3	0.249
MBLLEN [54]	76.3	0.086	63.0	0.332
DeepLPE [57]	76.3	0.138	61.9	0.807
Zero-DCE [24]	76.9	0.042	61.9	0.300
MAET (w ort) [14]	74.0	0.123	-	-
IAT [13]	77.2	0.040	62.1	0.280
ILE-YOLO [81]	78.5	0.047	64.3	0.306
ExpoMamba	79.8	0.076	64.3	0.297

Loss Function. We use a multi-term loss to supervise both low-level fidelity and perceptual realism during training: $\mathbf{L} = \alpha \mathbf{L}_{l1} + \beta \mathbf{L}_{vgg} + \gamma \mathbf{L}_{ssim} + \delta \mathbf{L}_{lpips}$

Ablation Study. We have performed an ablation study of our ExpoMamba model over the LOL-v1 dataset. The standard convolutional block in U-Net/M-Net architecture was replaced with DoubleConv block. Block refers to the residual block used in each upsampling stage. We explored three HDR variants: HDR and HDR_{out}, which use a single HDR layer placed at different locations, and HDR-CSRNet+, a deeper network originally designed for congested scene recognition and used within FSSB.

The results show that DoubleConv and FSSB contribute most significantly to performance, with FSSB alone improving PSNR to 22.459. The inclusion of residual blocks and the DA module further enhances quality. Among HDR variants, HDR-CSRNet+ achieves the highest gains, reaching 25.640 PSNR and 0.860 SSIM, outperforming both HDR and HDR_{out}. Each component plays a key role in maximizing the effectiveness of ExpoMamba.

5. Human Evaluation

We performed a human study with 30 participants³ and 7 perceptual criteria⁴ beyond statistical metrics that may overlook perceptual aspects. Participants assessed the performance of various image enhancement models on ten diverse scenes, including varied objects, landscapes, and illuminance levels. See Figs. 5 and 6.

From Tab. 6, we picked four strong baselines: IAT [13], I-SID [30], FECNet [31], DRBN [91]. ExpoMamba meets or exceeds them (3.23 vs DRBN 3.27, FECNet 2.92, I-SID 2.88, IAT 2.73) Supp. Fig. 8, yet runs 2–3× faster and uses ~4× less memory. These findings support our “comparable quality, better efficiency” claim. Additional results in Appx. C.

³30 participants selected randomly from a pool of over 96,000 on the crowdsourcing platform Prolific.

⁴We assessed [3] each model’s naturalness, brightness, color, sharpness, detail, noise, and contrast to fully map its strengths and weaknesses.

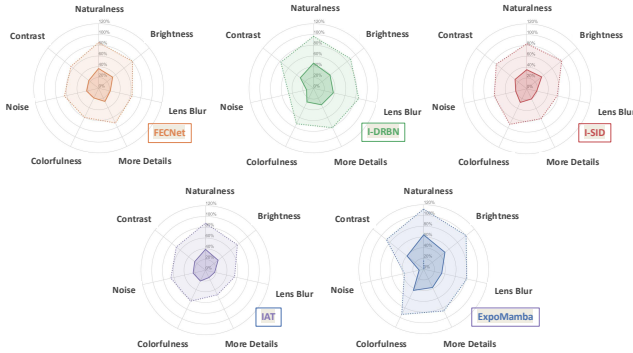


Figure 5. Perceptual evaluation results for ExpoMamba and baseline models (FECNet, I-DRBN, I-SID, and IAT) across key criteria. ExpoMamba demonstrates a balanced and robust performance, particularly excelling in brightness, reduced blur, and detail retention.

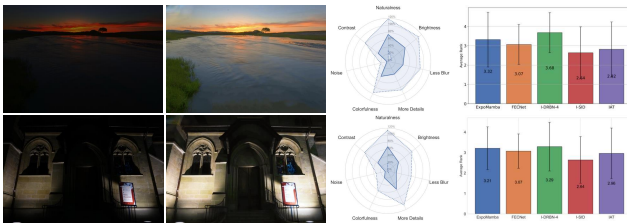


Figure 6. Outputs with corresponding spider charts and average rank rating in human evaluation. The images are selected from the test dataset as the top most diverse set of images showing varying lux values, mixed-exposure, varying color density.

6. Results

The performances in Tables 1, 2, 4, and 6. Tab. 1 compares ExpoMamba to 19 state-of-the-art baselines, including lightweight and heavy models. We evaluate performance using SSIM, PSNR, LPIPS, and FID. ExpoMamba_s achieves an inference time of **36 ms**, faster than most baselines (Fig. 1) and is the fastest among comparable models. Models like DiffLL [34], CIDNet [19], and LLformer [80] have comparable results but much higher inference times. Traditional algorithms (e.g., MSRCR [36], MF [20], BIMEF [92], SRIE [21], FEA [16], NPE [76], and LIME [26]) generally perform poorly on LOL4K (Tab. 2). Fig. 1.b shows that increasing image resolution to 4K significantly increases inference time for transformer models due to their quadratic complexity. Despite being a 41 million parameter model, ExpoMamba demonstrates remarkable storage efficiency, consuming $\sim 1/4^{th}$ memory (2923 Mb) compared to CIDNet, which, despite its smaller size of 1.9 million parameters, consumes 8249 Mb. This is because of ExpoMamba’s state expansion design, which aligns computation with the GPU’s high-bandwidth memory characteristics and removes the quadratic bottleneck, thereby reducing memory footprint. Current SOTA models CIDNet [19] and

LLformer [80] are slower and less memory-efficient.

Comparison with Mamba-based Methods. As detailed in Tab. 3, ExpoMamba significantly outperforms baselines across both datasets. These results validate our core architectural hypothesis: the explicit, decoupled modeling of amplitude and phase within our FSSB provides a more effective framework for LLIE than using Mamba as a general-purpose feature extractor.

Illuminating Real-World Downstream Tasks. To assess the real-world applicability of ExpoMamba, we evaluate its impact on downstream tasks using the ExDark dataset [52] and ACDC dataset [66]. Our downstream evaluations demonstrate that ExpoMamba not only produces perceptually improved images, but also enhances the operational accuracy of vision models in critical tasks of object detection and segmentation. This performance (with details shown in Tab. 4) suggests that *ExpoMamba* can serve as a robust preprocessing stage for machine-oriented pipelines, particularly in domains requiring vision reliability under poor illumination.

Analysis of Efficiency. A recurring question in evaluating modern architectures is the relationship between parameter count and computational speed. ExpoMamba_s (41M params) has a larger parameter count than some lightweight methods, yet we report significantly faster inference times (36ms). This apparent contradiction is resolved by examining architectural efficiency rather than parameter counts.

The primary speed advantage of ExpoMamba stems from the **linear-time complexity** ($O(N)$) of the underlying SSM, which fundamentally avoids the quadratic scaling bottleneck ($O(N^2)$) of self-attention in transformers. This advantage becomes particularly pronounced at high resolutions. Furthermore, our model is hardware-aware, leveraging optimized **kernel fusion** techniques that significantly reduce memory I/O overhead by a factor of 20-40× [22], which also contributes to its lower memory footprint compared to other models. Thus, while a higher parameter count provides the necessary model capacity for quality enhancement, it is the fundamental efficiency of the SSM architecture and its hardware-conscious implementation that deliver low-latency performance.

7. Conclusion

ExpoMamba combines frequency-based processing and state-space models to enhance low-light images, offering robust performance and efficiency for real-world applications like mobile devices and surveillance systems. Our extensive experiments, including comparisons with SOTA models and human perceptual studies, validate the superiority of our approach.

References

- [1] Eashan Adhikarla, Kai Zhang, Rosaura G. VidalMata, Manjushree Aithal, Nikhil Ambha Madhusudhana, John Nicholson, Lichao Sun, and Brian D. Davison. Unified-egformer: Exposure guided lightweight transformer for mixed-exposure image enhancement. In *Pattern Recognition*, pages 260–275, Cham, 2025. Springer Nature Switzerland. 1
- [2] Mahmoud Afifi, Konstantinos G Derpanis, Bjorn Ommer, and Michael S Brown. Learning multi-scale photo exposure correction. In *Proceedings of the IEEE/CVF Conference on Computer Vision and Pattern Recognition*, pages 9157–9167, 2021. 7
- [3] Manjushree Aithal, Rosaura G. VidalMata, Manikandantan Kartha, Gong Chen, Eashan Adhikarla, Lucas N. Kirsten, Zhicheng Fu, Nikhil A. Madhusudhana, and Joe Nasti. Lenviz: A high-resolution low-exposure night vision benchmark dataset, 2025. 7
- [4] Rayan Al Sobhahi and Joe Tekli. Low-light homomorphic filtering network for integrating image enhancement and classification. *Signal Processing: Image Communication*, 100:116527, 2022. 13
- [5] Jiesong Bai, Yuhao Yin, Qiyuan He, Yuanxian Li, and Xiaofeng Zhang. Retinexmamba: Retinex-based mamba for low-light image enhancement. In *International Conference on Neural Information Processing*, pages 427–442. Springer, 2025. 2, 6, 13
- [6] Alexandru Brateanu, Raul Balmez, Adrian Avram, and CC Orhei. Lyt-net: Lightweight yuv transformer-based network for low-light image enhancement. *arXiv preprint arXiv:2401.15204*, 2024. 2, 13
- [7] Jianrui Cai, Shuhang Gu, and Lei Zhang. Learning a deep single image contrast enhancer from multi-exposure images. *IEEE Transactions on Image Processing*, 27(4):2049–2062, 2018. 6, 7
- [8] Yuanhao Cai, Hao Bian, Jing Lin, Haoqian Wang, Radu Timofte, and Yulun Zhang. Retinexformer: One-stage retinex-based transformer for low-light image enhancement. In *Proceedings of the IEEE/CVF international conference on computer vision*, pages 12504–12513, 2023. 2
- [9] Hanting Chen, Yunhe Wang, Tianyu Guo, Chang Xu, Yiping Deng, Zhenhua Liu, Siwei Ma, Chunjing Xu, Chao Xu, and Wen Gao. Pre-trained image processing transformer. In *Proceedings of the IEEE/CVF conference on computer vision and pattern recognition*, pages 12299–12310, 2021. 1, 2, 13
- [10] Tianle Chen, Yu Li, and Xuedong Zhang. Mwrdr (mamba wavelet reverse diffusion)—an efficient fundus image enhancement network based on an improved state-space model. *Electronics*, 13(20):4025, 2024. 13
- [11] Yifan Chen, Qi Zeng, Heng Ji, and Yun Yang. Skyformer: Remodel self-attention with gaussian kernel and nystrom method. In *Advances in Neural Information Processing Systems*, pages 2122–2135. Curran Associates, Inc., 2021. 2
- [12] Yongbiao Chen, Sheng Zhang, Fangxin Liu, Zhigang Chang, Mang Ye, and Zhengwei Qi. Transhash: Transformer-based hamming hashing for efficient image retrieval. *CoRR*, abs/2105.01823, 2021. 2
- [13] Ziteng Cui, Kunchang Li, Lin Gu, Shenghan Su, Peng Gao, ZhengKai Jiang, Yu Qiao, and Tatsuya Harada. You only need 90k parameters to adapt light: a light weight transformer for image enhancement and exposure correction. In *33rd British Machine Vision Conference 2022, BMVC 2022, London, UK, November 21-24, 2022*. BMVA Press, 2022. 2, 6, 7, 13
- [14] Ziteng Cui, Guo-Jun Qi, Lin Gu, Shaodi You, Zenghui Zhang, and Tatsuya Harada. Multitask AET with orthogonal tangent regularity for dark object detection. *CoRR*, abs/2205.03346, 2022. 7
- [15] R Dale-Jones and Tardi Tjahjadi. A study and modification of the local histogram equalization algorithm. *Pattern Recognition*, 26(9):1373–1381, 1993. 1
- [16] Xuan Dong, Guan Wang, Yi Pang, Weixin Li, Jiangtao Wen, Wei Meng, and Yao Lu. Fast efficient algorithm for enhancement of low lighting video. In *ICME*, pages 1–6, 2011. 8
- [17] Alexey Dosovitskiy, Lucas Beyer, Alexander Kolesnikov, Dirk Weissenborn, Xiaohua Zhai, Thomas Unterthiner, Mostafa Dehghani, Matthias Minderer, Georg Heigold, Sylvain Gelly, Jakob Uszkoreit, and Neil Houlsby. An image is worth 16x16 words: Transformers for image recognition at scale. *ICLR*, 2021. 2
- [18] Feyza Duman Keles, Pruthuvi Mahesakya Wijewardena, and Chinmay Hegde. On the computational complexity of self-attention. In *Proceedings of The 34th International Conference on Algorithmic Learning Theory*, pages 597–619. PMLR, 2023. 2
- [19] Yixu Feng, Cheng Zhang, Pei Wang, Peng Wu, Qingsen Yan, and Yanning Zhang. You only need one color space: An efficient network for low-light image enhancement, 2024. 2, 8
- [20] Xueyang Fu, Delu Zeng, Yue Huang, Yinghao Liao, Xinghao Ding, and John Paisley. A fusion-based enhancing method for weakly illuminated images. *Signal Processing*, 129:82–96, 2016. 8
- [21] Xueyang Fu, Delu Zeng, Yue Huang, Xiao-Ping Zhang, and Xinghao Ding. A weighted variational model for simultaneous reflectance and illumination estimation. In *CVPR*, pages 2782–2790, 2016. 6, 8
- [22] Albert Gu and Tri Dao. Mamba: Linear-time sequence modeling with selective state spaces, 2023. 2, 4, 8, 13
- [23] Chunle Guo, Chongyi Li, Jichang Guo, Chen Change Loy, Junhui Hou, Sam Kwong, and Runmin Cong. Zero-reference deep curve estimation for low-light image enhancement. In *CVPR*, pages 1780–1789, 2020. 6
- [24] Chunle Guo Guo, Chongyi Li, Jichang Guo, Chen Change Loy, Junhui Hou, Sam Kwong, and Runmin Cong. Zero-reference deep curve estimation for low-light image enhancement. In *Proceedings of the IEEE conference on computer vision and pattern recognition (CVPR)*, pages 1780–1789, 2020. 7
- [25] Lanqing Guo, Chong Wang, Wenhan Yang, Siyu Huang, Yufei Wang, Hanspeter Pfister, and Bihan Wen. Shadowdiffusion: When degradation prior meets diffusion model for

- shadow removal. In *Proceedings of the IEEE/CVF Conference on Computer Vision and Pattern Recognition*, pages 14049–14058, 2023. 13
- [26] Xiaojie Guo, Yu Li, and Haibin Ling. Lime: Low-light image enhancement via illumination map estimation. *IEEE TIP*, 26(2):982–993, 2016. 8
- [27] Ziang Guo, Stepan Perminov, Mikhail Konenkov, and Dzmityr Tsetserukou. Hawkdrive: A transformer-driven visual perception system for autonomous driving in night scene. *arXiv preprint arXiv:2404.04653*, 2024. 1
- [28] Litao Hu, Huaijin Chen, and Jan P. Allebach. Joint multi-scale tone mapping and denoising for hdr image enhancement. In *2022 IEEE/CVF Winter Conference on Applications of Computer Vision Workshops (WACVW)*, pages 729–738, 2022. 5
- [29] Jie Huang, Zhiwei Xiong, Xueyang Fu, Dong Liu, and Zheng-Jun Zha. Hybrid image enhancement with progressive laplacian enhancing unit. In *Proceedings of the 27th ACM International Conference on Multimedia*, page 1614–1622, New York, NY, USA, 2019. Association for Computing Machinery. 7
- [30] Jie Huang, Yajing Liu, Xueyang Fu, Man Zhou, Yang Wang, Feng Zhao, and Zhiwei Xiong. Exposure normalization and compensation for multiple-exposure correction. In *Proceedings of the IEEE/CVF Conference on Computer Vision and Pattern Recognition*, pages 6043–6052, 2022. 7
- [31] Jie Huang, Yajing Liu, Feng Zhao, Keyu Yan, Jinghao Zhang, Yukun Huang, Man Zhou, and Zhiwei Xiong. Deep fourier-based exposure correction network with spatial-frequency interaction. In *European Conference on Computer Vision*, pages 163–180. Springer, 2022. 7
- [32] Jie Huang, Feng Zhao, Man Zhou, Jie Xiao, Naishan Zheng, Kaiwen Zheng, and Zhiwei Xiong. Learning sample relationship for exposure correction. In *Proceedings of the IEEE/CVF Conference on Computer Vision and Pattern Recognition*, pages 9904–9913, 2023. 7
- [33] Xun Huang and Serge Belongie. Arbitrary style transfer in real-time with adaptive instance normalization, 2017. 7
- [34] Hai Jiang, Ao Luo, Haoqiang Fan, Songchen Han, and Shuaicheng Liu. Low-light image enhancement with wavelet-based diffusion models. *ACM Transactions on Graphics (TOG)*, 42(6):1–14, 2023. 8, 16
- [35] Yifan Jiang, Xinyu Gong, Ding Liu, Yu Cheng, Chen Fang, Xiaohui Shen, Jianchao Yang, Pan Zhou, and Zhangyang Wang. Enlightengan: Deep light enhancement without paired supervision. *IEEE TIP*, 30:2340–2349, 2021. 6
- [36] Daniel J Jobson, Zia-ur Rahman, and Glenn A Woodell. A multiscale retinex for bridging the gap between color images and the human observation of scenes. *IEEE TIP*, 6(7):965–976, 1997. 6, 8
- [37] A. Katharopoulos, A. Vyas, N. Pappas, and F. Fleuret. Transformers are rnns: Fast autoregressive transformers with linear attention. In *Proceedings of the International Conference on Machine Learning (ICML)*, 2020. 1, 2
- [38] Mohammad Farhan Khan, Ekram Khan, and Zia Ahmad Abbasi. Segment dependent dynamic multi-histogram equalization for image contrast enhancement. *Digital Signal Processing*, 25:198–223, 2014. 1
- [39] Nikita Kitaev, Lukasz Kaiser, and Anselm Levskaya. Reformer: The efficient transformer. In *International Conference on Learning Representations*, 2020. 2
- [40] Edwin H Land and John J McCann. Lightness and retinex theory. *Josa*, 61(1):1–11, 1971. 1
- [41] Victor Lazzarini. *Frequency-Domain Techniques*, pages 223–271. Springer International Publishing, Cham, 2017. 3
- [42] Chongyi Li, Chunle Guo Guo, and Chen Change Loy. Learning to enhance low-light image via zero-reference deep curve estimation. In *IEEE Transactions on Pattern Analysis and Machine Intelligence*, 2021. 2, 6
- [43] Chongyi Li, Chun-Le Guo, Man Zhou, Zhexin Liang, Shangchen Zhou, Ruicheng Feng, and Chen Change Loy. Embedding fourier for ultra-high-definition low-light image enhancement. *arXiv preprint arXiv:2302.11831*, 2023. 6
- [44] Guanlin Li, Ke Zhang, Ting Wang, Ming Li, Bin Zhao, and Xuelong Li. Semi-llie: Semi-supervised contrastive learning with mamba-based low-light image enhancement. *arXiv preprint arXiv:2409.16604*, 2024. 2, 13
- [45] Orly Liba, Kiran Murthy, Yun-Ta Tsai, Tim Brooks, Tianfan Xue, Nikhil Karnad, Qiurui He, Jonathan T Barron, Dillon Sharlet, Ryan Geiss, et al. Handheld mobile photography in very low light. *ACM Trans. Graph.*, 38(6):164–1, 2019. 1
- [46] Seokjae Lim and Wonjun Kim. Dslr: Deep stacked laplacian restorer for low-light image enhancement. *IEEE TMM*, 23:4272–4284, 2020. 6
- [47] Jiaying Liu, Xu Deja, Wenhan Yang, Minhao Fan, and Haofeng Huang. Benchmarking low-light image enhancement and beyond. *International Journal of Computer Vision*, 129:1153–1184, 2021. 7
- [48] Liu Liu, Zheng Qu, Zhaodong Chen, Yufei Ding, and Yuan Xie. Transformer acceleration with dynamic sparse attention. *CoRR*, abs/2110.11299, 2021. 2
- [49] Risheng Liu, Long Ma, Jiao Zhang, Xin Fan, and Zhongxuan Luo. Retinex-inspired unrolling with cooperative prior architecture search for low-light image enhancement. In *CVPR*, pages 10561–10570, 2021. 6
- [50] Xiaoning Liu, Zongwei Wu, Ao Li, Florin-Alexandru Vasluianu, Yulun Zhang, Shuhang Gu, Le Zhang, Ce Zhu, Radu Timofte, Zhi Jin, et al. Ntire 2024 challenge on low light image enhancement: Methods and results. *arXiv preprint arXiv:2404.14248*, 2024. 1
- [51] Ying Liu. Design of a two-branch network enhancement algorithm for deep features in visually communicated images. *Signal, Image and Video Processing*, pages 1–12, 2024. 5
- [52] Yuen Peng Loh and Chee Seng Chan. Getting to know low-light images with the exclusively dark dataset. *Computer Vision and Image Understanding*, 178:30–42, 2019. 6, 8
- [53] Jiachen Lu, Jinghan Yao, Junge Zhang, Xiatian Zhu, Hang Xu, Weiguo Gao, Chunjing XU, Tao Xiang, and Li Zhang. Soft: Softmax-free transformer with linear complexity. In *Advances in Neural Information Processing Systems*, pages 21297–21309. Curran Associates, Inc., 2021. 2

- [54] Feifan Lv, Feng Lu, Jianhua Wu, and Chongsoon Lim. Mblen: Low-light image/video enhancement using cnns. In *British Machine Vision Conference (BMVC)*, 2018. 7
- [55] Long Ma, Tengyu Ma, Risheng Liu, Xin Fan, and Zhongxuan Luo. Toward fast, flexible, and robust low-light image enhancement. In *Proceedings of the IEEE/CVF Conference on Computer Vision and Pattern Recognition (CVPR)*, pages 5637–5646, 2022. 7
- [56] Raghav Mehta and Jayanthi Sivaswamy. M-net: A convolutional neural network for deep brain structure segmentation. In *2017 IEEE 14th international symposium on biomedical imaging (ISBI 2017)*, pages 437–440. IEEE, 2017. 2
- [57] Sean Moran, Pierre Marza, Steven McDonagh, Sarah Parisot, and Gregory Slabaugh. Deeplpf: Deep local parametric filters for image enhancement. In *Proceedings of the IEEE/CVF Conference on Computer Vision and Pattern Recognition (CVPR)*, 2020. 7
- [58] Chamin Morikawa, Michihiro Kobayashi, Masaki Satoh, Yasuhiro Kuroda, Teppei Inomata, Hitoshi Matsuo, Takeshi Miura, and Masaki Hilaga. Image and video processing on mobile devices: a survey. *the visual Computer*, 37(12): 2931–2949, 2021. 2
- [59] Shuwei Peng, Xu Zhang, Aiwen Jiang, Changhong Liu, and Jihua Ye. Low-light image enhancement via fourier-mamba: A hybrid frequency-spatial approach. In *Proceedings of the 6th ACM International Conference on Multimedia in Asia*, pages 1–8, 2024. 2, 6
- [60] Ashwini Pokle, Zhengyang Geng, and J Zico Kolter. Deep equilibrium approaches to diffusion models. *Advances in Neural Information Processing Systems*, 35:37975–37990, 2022. 13
- [61] Vaishnav Potlapalli, Syed Waqas Zamir, Salman Khan, and Fahad Khan. Promptir: Prompting for all-in-one image restoration. In *Thirty-seventh Conference on Neural Information Processing Systems*, 2023. 13
- [62] Xuebin Qin, Zichen Zhang, Chenyang Huang, Masood Dehghan, Osmar Zaiane, and Martin Jagersand. U2-net: Going deeper with nested u-structure for salient object detection. In *Pattern Recognition 2020*, page 107404, 2020. 2
- [63] Joseph Redmon and Ali Farhadi. Yolov3: An incremental improvement. *CoRR*, abs/1804.02767, 2018. 7
- [64] Xutong Ren, Wenhan Yang, Wen-Huang Cheng, and Jiaying Liu. Lr3m: Robust low-light enhancement via low-rank regularized retinex model. *IEEE Transactions on Image Processing*, 29:5862–5876, 2020. 1
- [65] Chitwan Saharia, William Chan, Huiwen Chang, Chris Lee, Jonathan Ho, Tim Salimans, David Fleet, and Mohammad Norouzi. Palette: Image-to-image diffusion models. In *ACM SIGGRAPH 2022 conference proceedings*, pages 1–10, 2022. 13
- [66] Christos Sakaridis, Dengxin Dai, and Luc Van Gool. ACDC: The adverse conditions dataset with correspondences for semantic driving scene understanding. In *Proceedings of the IEEE/CVF International Conference on Computer Vision (ICCV)*, 2021. 6, 8
- [67] Zhuoran Shen, Mingyuan Zhang, Haiyu Zhao, Shuai Yi, and Hongsheng Li. Efficient attention: Attention with linear complexities. In *IEEE Winter Conference on Applications of Computer Vision, WACV 2021, Waikoloa, HI, USA, January 3-8, 2021*, pages 3530–3538. IEEE, 2021. 1
- [68] Pooja Shrivastav. Advancements and challenges in low-light object detection. In *2024 2nd International Conference on Intelligent Data Communication Technologies and Internet of Things (IDCIoT)*, pages 1351–1356. IEEE, 2024. 1
- [69] Kuldeep Singh, Rajiv Kapoor, and Sanjeev Kr Sinha. Enhancement of low exposure images via recursive histogram equalization algorithms. *Optik*, 126(20):2619–2625, 2015. 1
- [70] Junhao Tan, Songwen Pei, Wei Qin, Bo Fu, Ximing Li, and Libo Huang. Wavelet-based mamba with fourier adjustment for low-light image enhancement. *arXiv preprint arXiv:2410.20314*, 2024. 2, 6, 13
- [71] Yi Tay, Mostafa Dehghani, Dara Bahri, and Donald Metzler. Efficient transformers: A survey. *ACM Comput. Surv.*, 55(6), 2022. 4
- [72] Chiheb Trabelsi, Olexa Bilaniuk, Ying Zhang, Dmitriy Serdyuk, Sandeep Subramanian, João Felipe Santos, Soroush Mehri, Negar Rostamzadeh, Yoshua Bengio, and Christopher J. Pal. Deep complex networks. In *6th International Conference on Learning Representations, ICLR 2018, Vancouver, BC, Canada, April 30 - May 3, 2018, Conference Track Proceedings*. OpenReview.net, 2018. 5
- [73] Zhengzhong Tu, Hossein Talebi, Han Zhang, Feng Yang, Peyman Milanfar, Alan Bovik, and Yinxiao Li. Maxim: Multi-axis mlp for image processing. In *Proceedings of the IEEE/CVF conference on computer vision and pattern recognition*, pages 5769–5780, 2022. 13
- [74] Haoyuan Wang, Ke Xu, and Rynson WH Lau. Local color distributions prior for image enhancement. In *European Conference on Computer Vision*, pages 343–359. Springer, 2022. 7
- [75] Ruixing Wang, Qing Zhang, Chi-Wing Fu, Xiaoyong Shen, Wei-Shi Zheng, and Jiaya Jia. Underexposed photo enhancement using deep illumination estimation. In *The IEEE Conference on Computer Vision and Pattern Recognition (CVPR)*, 2019. 7
- [76] Shuhang Wang, Jin Zheng, Hai-Miao Hu, and Bo Li. Naturalness preserved enhancement algorithm for non-uniform illumination images. *IEEE TIP*, 22(9):3538–3548, 2013. 8
- [77] Sinong Wang, Belinda Z. Li, Madian Khabisa, Han Fang, and Hao Ma. Linformer: Self-attention with linear complexity, 2020. 1
- [78] Shuang Wang, Qingchuan Tao, and Zhenming Tang. Resvmunetx: A low-light enhancement network based on vmamba. *arXiv e-prints*, pages arXiv-2407, 2024. 2, 13
- [79] Tao Wang, Kaihao Zhang, Ziqian Shao, Wenhan Luo, Björn Stenger, Tae-Kyun Kim, Wei Liu, and Hongdong Li. Lldiffusion: Learning degradation representations in diffusion models for low-light image enhancement. *CoRR*, abs/2307.14659, 2023. 1
- [80] Tao Wang, Kaihao Zhang, Tianrun Shen, Wenhan Luo, Bjorn Stenger, and Tong Lu. Ultra-high-definition low-light image enhancement: A benchmark and transformer-based

- method. In *Proceedings of the AAAI Conference on Artificial Intelligence*, pages 2654–2662, 2023. 1, 2, 6, 8, 13, 16
- [81] Xiaofeng Wang, Rentao Yang, Zhize Wu, Lingma Sun, Jia-shan Liu, and Le Zou. Ilenet: Illumination-modulated laplacian-pyramid enhancement network for low-light object detection. *Expert Systems with Applications*, 271: 126504, 2025. 6, 7
- [82] Yufei Wang, Yi Yu, Wenhan Yang, Lanqing Guo, Lap-Pui Chau, Alex C Kot, and Bihan Wen. Exposediffusion: Learning to expose for low-light image enhancement. *arXiv preprint arXiv:2307.07710*, 2023. 1, 13
- [83] Zhendong Wang, Xiaodong Cun, Jianmin Bao, and Jianzhuang Liu. Uformer: A general u-shaped transformer for image restoration. In *CVPR*, pages 17683–17693, 2022. 6
- [84] Ziyang Wang, Jian-Qing Zheng, Yichi Zhang, Ge Cui, and Lei Li. Mamba-unet: Unet-like pure visual mamba for medical image segmentation, 2024. 2
- [85] Chen Wei, Wenjing Wang, Wenhan Yang, and Jiaying Liu. Deep retinex decomposition for low-light enhancement. In *British Machine Vision Conference 2018, BMVC 2018, Newcastle, UK, September 3-6, 2018*, page 155. BMVA Press, 2018. 6, 7
- [86] Jiangwei Weng, Zhiqiang Yan, Ying Tai, Jianjun Qian, Jian Yang, and Jun Li. Mamballie: Implicit retinex-aware low light enhancement with global-then-local state space. *arXiv preprint arXiv:2405.16105*, 2024. 2, 6, 13
- [87] Wenhui Wu, Jian Weng, Pingping Zhang, Xu Wang, Wenhan Yang, and Jianmin Jiang. Uretinex-net: Retinex-based deep unfolding network for low-light image enhancement. In *2022 IEEE/CVF Conference on Computer Vision and Pattern Recognition (CVPR)*, pages 5891–5900, 2022. 7
- [88] Xiaoyu Xian, Qi Zhou, Jinghui Qin, Xiaojun Yang, Yin Tian, Yukai Shi, and Daxin Tian. Crose: Low-light enhancement by cross-sensor interaction for nighttime driving scenes. *Expert Systems with Applications*, page 123470, 2024. 1
- [89] Zhitao Xiao and Zhengxin Hou. Phase based feature detector consistent with human visual system characteristics. *Pattern Recognition Letters*, 25(10):1115–1121, 2004. 3, 4, 5
- [90] Wenhan Yang, Shiqi Wang, Yuming Fang, Yue Wang, and Jiaying Liu. From fidelity to perceptual quality: A semi-supervised approach for low-light image enhancement. In *IEEE/CVF Conference on Computer Vision and Pattern Recognition (CVPR)*, 2020. 6
- [91] Wenhan Yang, Shiqi Wang, Yuming Fang, Yue Wang, and Jiaying Liu. From fidelity to perceptual quality: A semi-supervised approach for low-light image enhancement. In *Proceedings of the IEEE/CVF conference on computer vision and pattern recognition*, pages 3063–3072, 2020. 7
- [92] Zhenqiang Ying, Ge Li, and Wen Gao. A bio-inspired multi-exposure fusion framework for low-light image enhancement. *arXiv preprint arXiv:1711.00591*, 2017. 8
- [93] Shuang Yuan, Jinjiang Li, Lu Ren, and Zheng Chen. Multi-frequency field perception and sparse progressive network for low-light image enhancement. *Journal of Visual Communication and Image Representation*, 100:104133, 2024. 13
- [94] Manzil Zaheer, Guru Guruganesh, Kumar Avinava Dubey, Joshua Ainslie, Chris Alberti, Santiago Ontañón, Philip Pham, Anirudh Ravula, Qifan Wang, Li Yang, and Amr Ahmed. Big bird: Transformers for longer sequences. In *Advances in Neural Information Processing Systems 33: Annual Conference on Neural Information Processing Systems 2020, NeurIPS 2020, December 6-12, 2020, virtual*, 2020. 2
- [95] Syed Waqas Zamir, Aditya Arora, Salman Khan, Munawar Hayat, Fahad Shahbaz Khan, and Ming-Hsuan Yang. Restormer: Efficient transformer for high-resolution image restoration. In *CVPR*, pages 5728–5739, 2022. 6
- [96] Qinsheng Zhang, Molei Tao, and Yongxin Chen. gddim: Generalized denoising diffusion implicit models. *arXiv preprint arXiv:2206.05564*, 2022. 13
- [97] Tongshun Zhang, Pingping Liu, Mengcen Cai, Zijian Zhang, Yubing Lu, and Qiuzhan Zhou. Bsmamba: Brightness and semantic modeling for long-range interaction in low-light image enhancement. *arXiv preprint arXiv:2506.18346*, 2025. 2, 13
- [98] Xuanqi Zhang, Haijin Zeng, Jinwang Pan, Qiangqiang Shen, and Yongyong Chen. Llemamba: Low-light enhancement via relighting-guided mamba with deep unfolding network. *arXiv preprint arXiv:2406.01028*, 2024. 2, 13
- [99] Xingpeng Zhang, Sijing Wu, Qiuli Wang, and Kaixin Wang. Effretmamba: A light-weight mamba for low-light image enhancement. *Circuits, Systems, and Signal Processing*, 2025. 2, 6, 13
- [100] Yonghua Zhang, Jiawan Zhang, and Xiaojie Guo. Kindingling the darkness: A practical low-light image enhancer. In *ACMMM*, pages 1632–1640, 2019. 6
- [101] Zhuoran Zheng and Jun Zhang. Fd-vision mamba for endoscopic exposure correction, 2024. 3, 13
- [102] Dewei Zhou, Zongxin Yang, and Yi Yang. Pyramid diffusion models for low-light image enhancement. *arXiv preprint arXiv:2305.10028*, 2023. 1, 13
- [103] Man Zhou, Jie Huang, Chongyi Li, Hu Yu, Keyu Yan, Naisihan Zheng, and Feng Zhao. Adaptively learning low-high frequency information integration for pan-sharpening. In *Proceedings of the 30th ACM International Conference on Multimedia*, pages 3375–3384, 2022. 3
- [104] Man Zhou, Jie Huang, Chun-Le Guo, and Chongyi Li. Fourmer: An efficient global modeling paradigm for image restoration. In *International Conference on Machine Learning*, pages 42589–42601. PMLR, 2023. 1, 2, 3, 5, 13
- [105] Lianghui Zhu, Bencheng Liao, Qian Zhang, Xinlong Wang, Wenyu Liu, and Xinggang Wang. Vision mamba: Efficient visual representation learning with bidirectional state space model. *arXiv preprint arXiv:2401.09417*, 2024. 2, 4, 13
- [106] Wenbin Zou, Hongxia Gao, Weipeng Yang, and Tongtong Liu. Wave-mamba: Wavelet state space model for ultra-high-definition low-light image enhancement. In *Proceedings of the 32nd ACM International Conference on Multimedia*, pages 1534–1543, 2024. 2, 13

Appendix

A. Additional Related Work

Mamba Models. The emergence of mamba [22, 105] has catalyzed a new wave of innovation in low-light image enhancement (LLIE), with new architectures often building upon established theoretical frameworks. A significant portion of initial models are retinex inspired, integrating Mamba as a powerful and efficient engine for image decomposition and restoration. Pioneering works like Retinex-Mamba [5] demonstrated mamba’s viability by replacing computationally heavy transformer blocks to achieve greater efficiency. This was extended by LLEMamba [98], which embeds mamba within a deep unfolding network corresponding to an ADMM optimization algorithm, making the enhancement process both interpretable and context-aware. Other models like MambaLLIE [86] address the “local pixel forgetting” artifact of 1-D scanning by augmenting their state-space modules with local convolutions. Meanwhile, EffRetMamba [99] prioritizes speed by using jump-sampling to process a shorter sequence of image tokens, trading some information fidelity for a significant boost in inference time.

A second category of Mamba-based models moves beyond simple backbone replacement to propose novel interaction and learning paradigms. The most radical of these is BSMamba [97], which discards conventional spatial scanning entirely. Instead, it reorders image patches based on brightness and semantic content before the 1-D scan, allowing the model to establish long-range dependencies between functionally related but spatially distant pixels. Other models focus on alternative enhancement strategies or learning frameworks. ResVMUNetX [78], for example, opts for maximum efficiency by training a Mamba network to predict a simple additive residual map, enabling real-time video enhancement. Semi-LLIE [44] tackles the practical challenge of data scarcity, using a semi-supervised framework with a mamba backbone to effectively leverage vast amounts of unlabeled data. These diverse approaches highlight the versatility of the Mamba architecture and underscore a key trend: the most successful models are not naive, drop-in replacements, but are thoughtfully designed to synergize mamba’s strengths with domain-specific knowledge and innovative learning strategies.

Transformer Models. Transformer-based methods have been widely used for low-light enhancement due to their ability to model long-range dependencies. LLFormer [80] uses global attention to handle illumination inconsistencies. IAT [13] adapts lightweight transformer blocks for exposure correction. IPT [9] employs multi-task pretraining across restoration tasks using a shared transformer backbone. Fourmer [104] integrates Fourier transforms for improved global modeling. LYT-Net [6] leverages the YUV color

Table 7. Descriptions of two variants of our model, s' and l' , representing small and large model configurations.

Model Type	Configuration				Inference	Memory
	base channel	patch size	depth	params	speed	consumption
ExpoMamba _s	48	4	1	41 M	36 ms	2923 Mb
ExpoMamba _l	96	6	4	166 M	95.6 ms	5690 Mb

space for resource-efficient enhancement. MAXIM [73] introduces multi-axis gated MLPs for spatial and channel modeling. While effective, these models often incur high memory usage and quadratic runtime, making them less suited for real-time or mobile deployment.

Diffusion Models. Diffusion models have shown great potential in generating realistic and detailed images. The ExposureDiffusion model [82] integrates a diffusion process with a physics-based exposure model, enabling accurate noise modeling and enhanced performance in low-light conditions. Pyramid Diffusion [102] addresses computational inefficiencies by introducing a pyramid resolution approach, speeding enhancement without sacrificing quality. [65] handles image-to-image tasks using conditional diffusion processes. Models like [96] and deep non-equilibrium approaches [60] aim to reduce sampling steps for faster inference. However, starting from pure noise in conditional image restoration tasks remains a challenge for maintaining image quality while cutting down inference time [25].

Hybrid Modeling. Hybrid models include learning features in both spatial and frequency domains have been another popular area in image enhancement/restoration tasks. It has been predominantly explored in three sub-categories: (1) Fourier Transform [93], Fourmer [104], FD-VisionMamba [101]; (2) Wavelet Transform [10, 70, 106]; and, (3) Homomorphic Filtering [4]. Such methods demonstrate that leveraging both spatial and frequency information can significantly improve enhancement performance. Recent hybrid models such as MAXIM [73] and PromptIR [61] have explored lightweight but flexible design spaces for image restoration and enhancement tasks.

B. Extended Details on Phase Manipulation

This section provides a step-by-step derivation of how a uniform phase shift in the Fourier domain affects an image in the spatial domain.

We begin with the definition of the 2D Fourier Transform for an image $I(x, y)$:

$$\mathbf{F}(u, v) = \mathcal{F}\{I(x, y)\} = \iint_{-\infty}^{\infty} I(x, y)e^{-i2\pi(ux+vy)} dx dy \tag{10}$$

The transform can be represented in polar form using its amplitude $\mathbf{A}(u, v)$ and phase $\phi(u, v)$:

$$\mathbf{F}(u, v) = \mathbf{A}(u, v)e^{i\phi(u, v)} \tag{11}$$

The original image $I(x, y)$ is recovered via the Inverse Fourier Transform:

$$I(x, y) = \mathcal{F}^{-1}\{\mathbf{F}(u, v)\} = \iint_{-\infty}^{\infty} \mathbf{F}(u, v) e^{i2\pi(ux+vy)} du dv \quad (12)$$

Substituting the polar form into the inverse transform gives:

$$I(x, y) = \iint_{-\infty}^{\infty} \mathbf{A}(u, v) e^{i\phi(u, v)} e^{i2\pi(ux+vy)} du dv \quad (13)$$

Our goal is to analyze the effect of applying a uniform phase shift, $\Delta\phi$, to the phase component, resulting in a new phase $\phi'(u, v) = \phi(u, v) + \Delta\phi$. The modified Fourier spectrum is $\mathbf{F}'(u, v) = \mathbf{A}(u, v) e^{i(\phi(u, v) + \Delta\phi)}$. The corresponding image in the spatial domain, $I'(x, y)$, is derived as follows.

$$I'(x, y) = \iint \mathbf{A}(u, v) e^{i(\phi(u, v) + \Delta\phi)} e^{i2\pi(ux+vy)} du dv \quad (14)$$

$$= \iint \mathbf{A}(u, v) e^{i\phi(u, v)} e^{i\Delta\phi} e^{i2\pi(ux+vy)} du dv \quad (15)$$

$$= e^{i\Delta\phi} \iint \mathbf{A}(u, v) e^{i\phi(u, v)} e^{i2\pi(ux+vy)} du dv \quad (16)$$

$$= e^{i\Delta\phi} \cdot I(x, y) \quad (17)$$

$$= (\cos(\Delta\phi) + i \sin(\Delta\phi)) \cdot I(x, y) \quad (18)$$

$$= \cos(\Delta\phi)I(x, y) + i \sin(\Delta\phi)I(x, y) \quad (19)$$

In this derivation: Eq. (15) uses the exponential identity $e^{a+b} = e^a e^b$; Eq. (16) factors out the constant phase shift $\Delta\phi$ from the integral; Eq. (17) recognizes the inverse Fourier transform of the original image; Eq. (18) applies Euler’s formula $e^{i\theta} = \cos\theta + i \sin\theta$. Finally, Eq. (19) shows that a uniform phase shift in the frequency domain results in a complex-valued image where the real and imaginary parts are scaled versions of the original. This final expression (19) demonstrates that a uniform phase shift in the frequency domain results in multiplying the original image $I(x, y)$ by a complex constant $e^{i\Delta\phi}$. The new image $I'(x, y)$ is a complex-valued signal where the real part is the original image scaled by $\cos(\Delta\phi)$, and the imaginary part is the original image scaled by $\sin(\Delta\phi)$. This rotation in the complex plane fundamentally alters the image’s spatial characteristics, underscoring the critical role of phase information in defining structural content.

C. Additional Human Evaluation Results

As an extension to the main paper’s perceptual study, we present qualitative results and statistical rankings from our

Figure 7. Additional results from the SICE test set for human evaluation (continued from Fig. 6), along with corresponding spider charts and average rank ratings.

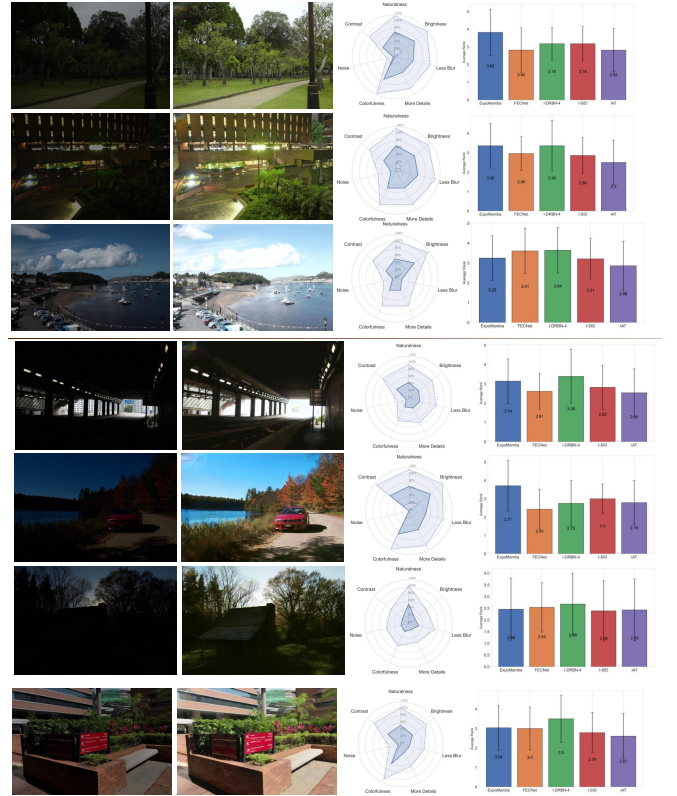
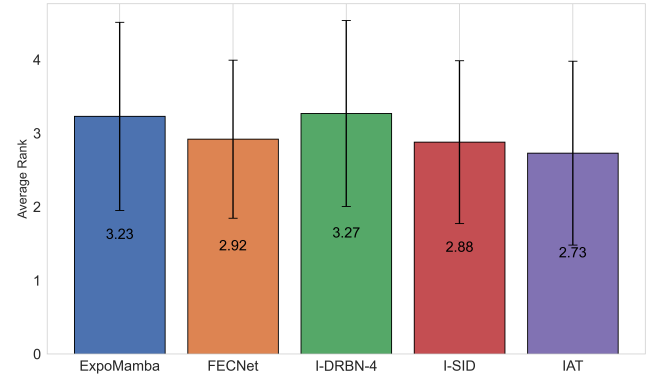


Figure 8. Aggregate rank comparison of ExpoMamba and baselines from human perceptual evaluation. Higher values indicate better subjective quality; error bars represent standard deviation.



human evaluation conducted on the SICE test dataset. Participants rated multiple image enhancement models across seven visual attributes: *naturalness*, *brightness*, *colorfulness*, *reduced blur*, *more details*, *noise reduction*, and *contrast*. In the spider charts (Fig. 7), ExpoMamba consistently outperforms competing methods across all criteria, with es-

pecially strong scores in the *noise reduction*, *naturalness*, and *detail retention* dimensions.

The aggregated average ranks across all images and participants are summarized in Fig. 8. ExpoMamba receives the highest overall perceptual ranking, demonstrating its ability to deliver visually balanced and subjectively preferred results. The small standard deviation further reflects strong inter-rater consistency, reinforcing the perceptual robustness of the proposed method.

D. Frequency-Dependent Dynamic Adaptation.

Let $r(u, v) = \frac{\sqrt{u^2+v^2}}{r_{\max}}$ denote the normalized radial frequency. We parameterize frequency dependent state matrices via shallow gating functions $\alpha_A(r)$, $\alpha_B(r)$, $\alpha_C(r)$ produced by a 1 layer MLP with Softplus, shared across channels:

$$\alpha_{\bullet}(r) = \log\left(1 + \exp\left(\mathbf{w}_{\bullet 2} \text{ReLU}(\mathbf{w}_{\bullet 1} r + b_{\bullet 1}) + b_{\bullet 2}\right)\right).$$

where, $\bullet \in \{A, B, C\}$. For each step t and frequency bin (u, v) , we form

$$\begin{aligned} A_t(u, v) &= A_t \circ (1 + \alpha_A(r(u, v))), \\ B_t(u, v) &= B_t \circ (1 + \alpha_B(r(u, v))), \\ C_t(u, v) &= C_t \circ (1 + \alpha_C(r(u, v))). \end{aligned}$$

Here, \circ denotes element wise multiplication. This keeps the SSM core intact while allowing smooth low to high frequency reweighting with three learnable gates. After separate processing through state-space models, the modified amplitude $\mathbf{A}''(\mathbf{u}, \mathbf{v})$ and phase $\mathbf{P}''(\mathbf{u}, \mathbf{v})$ are recombined and transformed back into the spatial domain to reconstruct the enhanced image: $\mathbf{I}'(\mathbf{x}, \mathbf{y}) = \mathbf{F}^{-1}(\mathbf{A}''(\mathbf{u}, \mathbf{v}) + i \cdot \mathbf{P}''(\mathbf{u}, \mathbf{v}))$; where, \mathbf{F}^{-1} denotes the inverse Fourier Transform.

E. Dynamic Patch Training

To improve robustness to variable input resolutions, ExpoMamba adopts a dynamic patch training strategy, as shown in Fig. 9. Specifically:

- In each training batch, a random patch size is selected from $\{128^2, 256^2, 324^2\}$.
- Each mini-batch contains images of the same resolution, but resolution varies across batches.
- The 2D scanning mechanism within FSSB is thereby trained to handle multi-scale representations efficiently.

This improves generalization to real-world conditions, especially on mobile devices and webcams that adapt resolution dynamically to conserve power or bandwidth.

F. Dynamic Adjustment Approximation

The Dynamic Adjustment Approximation (DAA) module provides an unsupervised mechanism for exposure correction by leveraging intrinsic image statistics, eliminating the

need for reference ground truth maps or pre-computed illumination priors. Unlike prior approaches such as KinD, LLFlow, or RetinexFormer, which rely heavily on ground-truth mean score as guidance signals derived from paired datasets, our method is entirely self-reliant and dynamically adapts to the brightness characteristics of each input. This approach helps in boosting the performance during inference.

Given an input image $\mathbf{I} \in \mathbb{R}^{C \times H \times W}$, we compute two summary statistics across all pixels and channels: the mean μ and the median m . A normalized intensity value $\tau \in [0, 1]$ is selected as the desired luminance anchor (empirically $\tau = 0.345$ in our case). The goal is to shift the median pixel values toward this anchor in a manner weighted by their deviation from the image’s current mean brightness.

The adjustment factor \mathbf{F} is computed as:

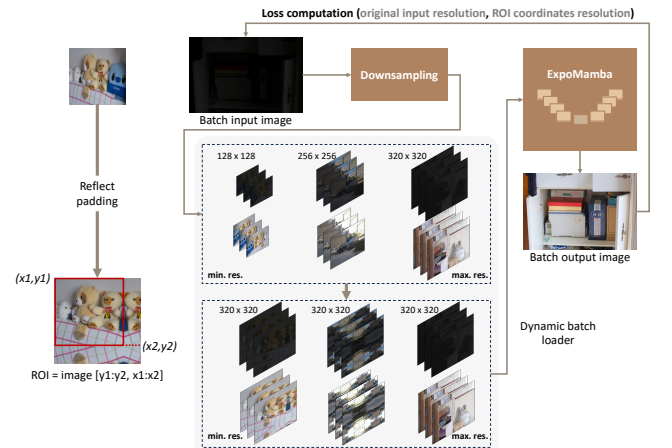
$$\mathbf{F} = \frac{m + \alpha \cdot (\tau - \mu)}{m} \quad (20)$$

Here, α is a tunable strength parameter that controls the degree of adjustment applied per image. The final adjusted image $\hat{\mathbf{I}}$ is computed element-wise as:

$$\hat{\mathbf{I}} = \mathbf{I} \times \mathbf{F} \quad (21)$$

This formulation ensures stability even under extreme low-light conditions by avoiding division by near-zero values and maintains exposure balance without introducing unnatural contrast. Because the adjustment is performed in a single-pass, the method is highly efficient and can be seamlessly integrated into real-time inference pipelines. Its effectiveness is especially pronounced in deployment scenarios where reference illumination statistics are unavailable, such as mobile or embedded imaging systems.

Figure 9. Illustration of dynamic patch training: multiple resolutions are randomly batched with padding, enabling the model to generalize across scales.



G. Additional Benchmark Visualizations

Fig. 10 illustrates additional visual comparisons across 16 baseline methods and the proposed ExpoMamba model. While methods such as Zero-DCE++, RUAS, and LIME tend to either over-enhance or introduce unnatural hues, ExpoMamba preserves both local structure and global illumination. Compared to LLFormer and Restormer, which occasionally oversmooth textures or lose highlight fidelity, ExpoMamba maintains sharper edges and natural luminance transitions. These results further validate the model’s ability to generalize well across diverse lighting conditions present in the LOLv1 dataset.

H. Discussion: Inference Time vs. FLOPs

In this work, we prioritize reporting real inference time over theoretical FLOPs, as the former provides a more accurate reflection of practical deployment efficiency. While FLOPs serve as a platform-agnostic metric for algorithmic complexity, they fail to capture critical system-level considerations such as memory bandwidth, caching behavior, and inter-layer communication, all of which play a substantial role in runtime performance on real hardware. In contrast, actual inference time directly reflects the influence of design choices such as data flow optimization, activation reuse, and parallel execution scheduling.

This distinction becomes especially important in latency-sensitive applications like augmented reality, autonomous navigation, or mobile imaging, where wall-clock latency, not theoretical compute, determines responsiveness and usability. For ExpoMamba, we report inference time measured on an NVIDIA A10G GPU, which accounts for the full end-to-end processing pipeline, including frequency decomposition, dual VSSM inference, and reconstruction. This emphasis on timing enables a fairer and more relevant comparison with baseline models in the context of deployment scenarios.

Optimizing for real-time execution rather than abstract operation counts ensures that ExpoMamba is not only computationally efficient but also pragmatically viable for edge environments where latency, memory, and energy constraints coexist.

I. Extended Comparative Efficiency and Model Scalability

Comparative Efficiency Analysis. ExpoMamba achieves a strong balance between visual quality and practical deployment metrics. As reported in Tab. 1, it processes a 400×600 image in 36 ms with a 2923 MB memory footprint—substantially faster than DiffLL [34] (158 ms, 8249 MB) and LLFormer [80] (1956 ms, 6 GB). This performance highlights the advantage of using linear-time operations and frequency-state modeling over transformer-based alternatives for real-time applications.

Balancing Speed and Effectiveness. Although ExpoMamba is not the smallest model in terms of parameter count, it outperforms many smaller baselines (e.g., IAT: 0.09M, FECNet+ERL: 0.15M) in both perceptual enhancement and downstream task accuracy (Tab. 4). Its modular architecture supports scalable deployment: ExpoMamba_s offers a lightweight configuration for edge devices, while ExpoMamba_l can scale up for cloud or desktop inference. This adaptability—combined with low latency and generalization across tasks—makes it a strong candidate for real-world LLIE pipelines in mobile, surveillance, and automotive domains.

J. Expanded Algorithm for ExpoMamba

Algorithm 2 ExpoMamba Training with Frequency State Space Block (FSSB)

```
1: Input: Dataset  $\mathcal{D}$ , Training epochs  $E$ , Components: FSSB, VSSMA, VSSMP, HDR, ComplexConv
2: Output: Optimized model parameters  $\theta$ 
3: // Frequency Decomposition
4: for each image  $I \in \mathcal{D}$  do
5:   Compute Fourier Transform  $\mathcal{F}(u, v) = \mathcal{F}[I(x, y)]$ 
6:   Decompose:  $\mathcal{F}(u, v) \rightarrow A(u, v), P(u, v)$ 
7: end for
8: // Frequency-State Modeling (FSSB)
9: for each component  $(u, v)$  do
10:   Update VSSMs:
11:      $\mathbf{h}[t+1] = \mathbf{A}[t] \cdot \mathbf{h}[t] + \mathbf{B}[t] \cdot \mathbf{x}[t], \mathbf{y}[t] = \mathbf{C}[t] \cdot \mathbf{h}[t]$ 
12:   Generate modulated outputs  $A''(u, v), P''(u, v)$ 
13: end for
14: // Inverse Transform & Reconstruction
15: Combine frequency outputs:  $\hat{\mathcal{F}}(u, v) = A''(u, v) + i \cdot P''(u, v)$ 
16: Apply Inverse Fourier Transform:  $\hat{I}(x, y) = \mathcal{F}^{-1}[\hat{\mathcal{F}}(u, v)]$ 
17: // Model Training
18: for  $e = 1$  to  $E$  do
19:   for each batch  $\mathcal{B} \subset \mathcal{D}$  do
20:     Pass  $\mathcal{B}$  through FSSB  $\rightarrow$  HDR  $\rightarrow$  ComplexConv
21:     Compute loss  $\mathcal{L}$ ; Backpropagate  $\nabla_{\theta} \mathcal{L}$ 
22:   end for
23: end for
24: Return: Trained parameters  $\theta$ 
```

K. Model Configuration.

Model configuration (see Table 7 for details) provides a detailed comparison between the two variants of ExpoMamba, highlighting their configurations and performance metrics. Notably, despite an increase of 125 million parameters, the memory of the larger ExpoMamba_l variant is 5690 Mb, which is a modest increase compared to transformer-based models and ExpoMamba_s.

Figure 10. Qualitative comparison of ExpoMamba and baselines on the LOLv1 dataset. Results demonstrate structural fidelity and color balance under mixed lighting conditions.

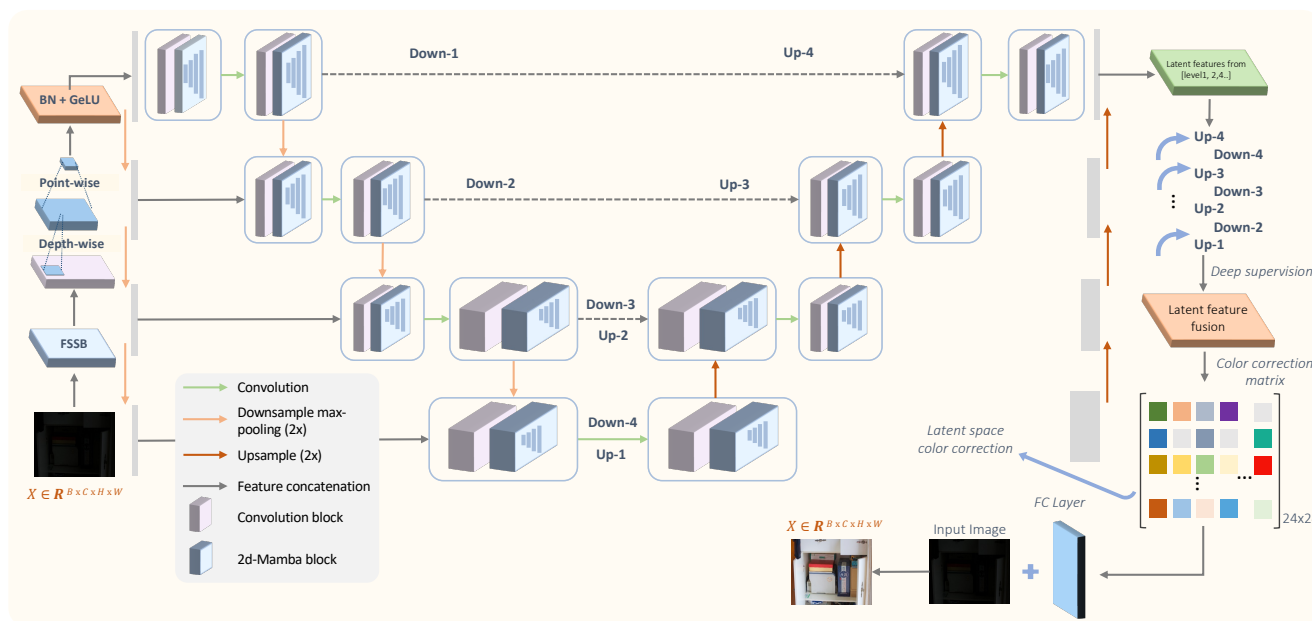
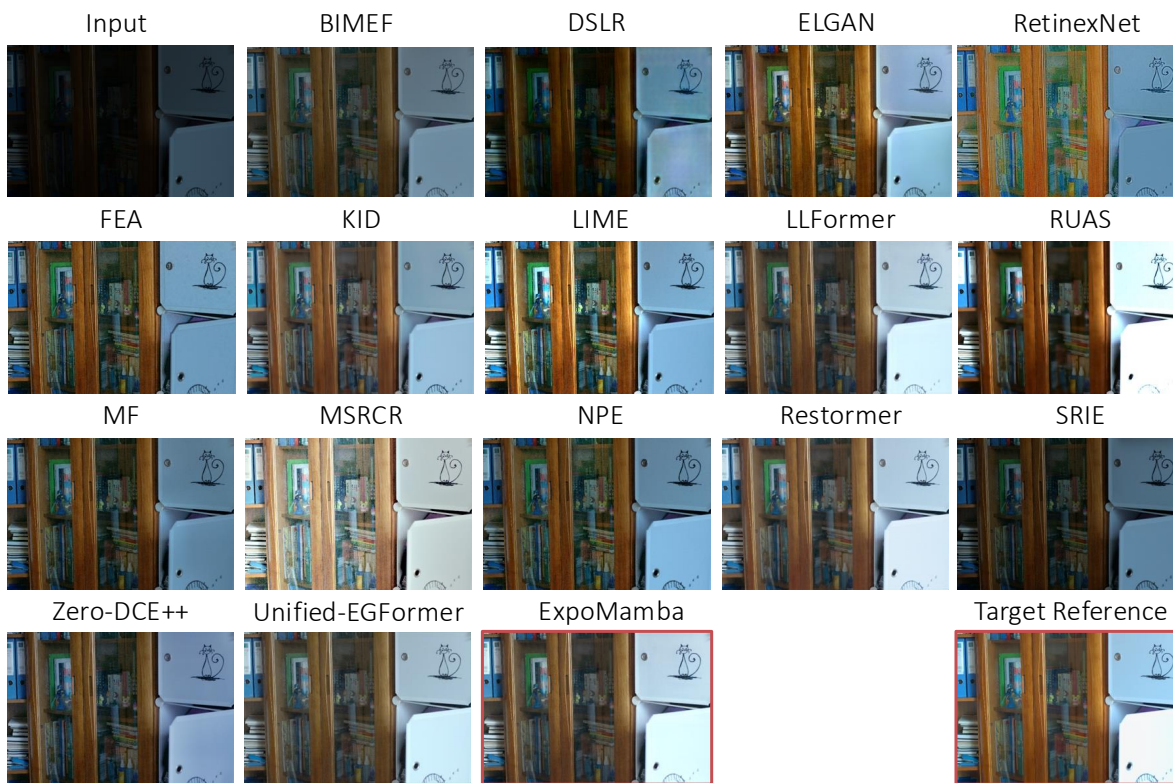


Figure 11. Overview of the ExpoMamba Architecture. The diagram illustrates the information flow through the *ExpoMamba* model.